This is the Pre-Published Version.

The following publication Feng, Y., Xu, W., Huang, B., Shao, Q., Xu, L., Yang, S., & Huang, X. (2019). On-demand, ultraselective hydrogenation system enabled by precisely modulated Pd–Cd nanocubes. Journal of the American Chemical Society, 142(2), 962-972 is available at https://doi.org/10.1021/jacs.9b10816.

This document is the Accepted Manuscript version of a Published Work that appeared in final form in Journal of the American Chemical Society, copyright © 2019 American Chemical Society after peer review and technical editing by the publisher

SELECTIVE HYDROGENATION

On-demand, ultraselective hydrogenation system enabled by precisely modulated Pd-Cd nanocubes

Yonggang Feng,[1#] Weiwei Xu,[2#] Bolong Huang,[3#] Qi Shao,[1] Lai Xu,[2*] Shuxing Bai,[1] Shize Yang,[4] Xiaoqing Huang[1*]

[1]College of Chemistry, Chemical Engineering and Materials Science, Soochow University, Jiangsu, 215123, China;

[2]Institute of Functional Nano & Soft Materials (FUNSOM), Jiangsu Key Laboratory for Carbon-Based Functional Materials and Devices, Soochow University, Jiangsu 215123, China;

[3]Department of Applied Biology and Chemical Technology, The Hong Kong Polytechnic University, Hung Hom, Kowloon, Hong Kong SAR.

[4]Center for Functional Nanomaterials, Brookhaven National Laboratory, Upton, New York 11973, United States.

[#]These authors contributed equally.

*Correspondence to: xulai15@suda.edu.cn; hxq006@suda.edu.cn

SUMMARY SENTENCE

High-performance selective hydrogenation was enabled by precisely modulated Pd-Cd nanocubes.

ABSTRACT

The pursuit of efficient hydrogenation nanocatalysts with an ultrahigh selectivity towards intricate substrates is state-of-the-art research but remains a formidable challenge. Herein, we report a series of novel $PdCd_x$ nanocubes (NCs) for the ultraselective hydrogenation reactions with flexible tuning feature . Obtaining a desirable conversion level of the substrates (e.g., 4-nitrophenylacetylene (NPA), 4-

nitrobenzaldehyde (NBAD) and 4-nitrostyrene (NS)) and competitive selectivity for all potential hydrogenation products have been achieved one by one under optimized hydrogenation conditions. The performance of these PdCdx NCs displays an evident dependence on both the composition and the use of Cd and a need for a distinct hydrogen source (H_2 or $HCOONH_4$). Additionally, for the selectivity of hydrogen to be suitably high, the morphology of the nano-cubes has a very well-defined effect. Density functional theory calculations confirmed the variation of adsorption energy for the substrate and hydrogenation products by carefully controlled introduction of Cd, leading to a desirable level of selectivity for all potential hydrogenation products. The $PdCd_x$ NCs also exhibit excellent reusability with negligible activity/selectivity decay and structural/composition changes after consecutive reactions. The present study provides advanced strategy for the rational design of superior hydrogenation nanocatalysts to achieve a practical application for highly desirable and selective hydrogenation reaction efficiency.

INTRODUCTION

Selectivity is fundamental to heterogeneous hydrogenation and is of great scientific and industrial interest (*1-3*). Currently, noble metals (e.g., Pd and Pt) that can readily activate hydrogen (H_2) are the best choice for the hydrogenation of unsaturated hydrocarbons (*2, 4-6*). Unfortunately, precise control of the further hydrogenation of the desirable product over bare noble metals is challenging, which usually results in a low selectivity. In general, a highly selective noble-metal nanocatalyst should primarily hydrogenate the reactant whilst avoiding consecutive hydrogenation of the desired product. In fact, the hydrogenation selectivity of noble metals can be encouraged by the introduction of a second metal or organic/inorganic compound (*7-16*), since this can lower the hydrogen dissociation ability of the active noble metal and reduce the binding energy of the desired products on nanocatalysts. However, with previously reported nanocatalysts, it remains a difficult task to selectively reduce the substrate with multiple unsaturated functional groups (e.g., alkynes, alkenes, aldehydes and nitroarene) while obtaining potential hydrogenation products with a desired selectivity (*4, 6, 17*). Nevertheless, achieving highly selective hydrogenation in the presence of competing unsaturated functional groups is of a great importance to the

pharmaceutical and chemical industry because many specific hydrogenation products are difficult to produce by simple organic synthesis (*18, 19*). Therefore, it is a highly desirable yet formidable challenge to achieve a sufficient level of selectivity of intricate substrates to on-demand hydrogenation products.

To achieve precise hydrogenation performance, the nature of the nanocatalyst (size, compositions and morphology, etc.) must be carefully controlled, which provides an ensemble control of the adsorption of hydrogenation sources, reactants and products (*20-25*). Here in this work, we have introduced Cd into Pd to form $PdCd_x$ as a potential electrocatalyst for the hydrogenation performance based on flexible control of compositions. We have developed a series of $PdCd_x$ nanocubes (NCs) (x = 0.53, 0.67, 0.82 and 1.13) for the selective hydrogenation of 4-nitrophenylacetylene (NPA) with both nitro and alkynyl groups. Remarkably, a highly desirable level of selectivity with a switchable feature for all five potential hydrogenation products, and an excellent reusability have been achieved over these systematically tuned $PdCd_x$ NCs under optimal hydrogenation conditions. The detailed theoretical study revealed that the tuning of the adsorption energy for the substrate and hydrogenation products by the precise introduction of Cd plays a key role in their obtaining a competitive selectivity. Significantly, the outstanding hydrogenation performance of $PdCd_x$ NCs can be readily applied to other intricate substrates (i.e., 4-nitrobenzaldehyde (NBAD) and 4-nitrostyrene (NS)), making it a practical potential hydrogenation nanocatalyst system with a very competitive selectivity for fine chemicals and beyond.

RESULTS AND DISCUSSION

A series of $PdCd_x$ NCs were successfully prepared through a facile wet-chemical approach, where the compositions of $PdCd_x$ NCs can be readily realized by tuning the amount of Cd precursor supplied while keeping the amount of Pd precursor constant (see Materials and Methods). To achieve better control over the Pd-Cd nanostructure, a variety of synthetic parameters were optimized. We found that the proper amount of reducing agent and use of oleic acid (OA) are essential for the preparation of well-defined PdCd NCs (**figs. S1 and S2**). The representative high-angle annular dark-field scanning transmission electron microscope (HAADF-STEM) image shows that the $PdCd_{0.82}$ NCs are fairly uniform in term of size and

shape, with an average edge length of 10.8 nm (**Fig. 1A**). The composition of the $PdCd_{0.82}$ NCs was determined to be Pd:Cd = 55.1:44.9 by using an energy dispersive X-ray spectrophotometer (EDS), which is consistent with results from inductively coupled plasma atomic emission spectroscopy (ICP-AES, Pd:Cd = 55.4:44.6) (**fig. S3**). As **Fig. 1B** shows, all the peaks of the powder X-ray diffraction (PXRD) pattern can be indexed to a body-center unit cell, where the 2θ values of 39.1°, 42.5°, 50.4°, 61.7° 68.0°, 75.6° and 83.2° can be indexed to the diffraction of the (111), (200), (002), (220), (202), (311) and (222) planes of PdCd, respectively (JCPDS file no. 06-0570). The crystalline nature of the $PdCd_{0.82}$ NCs was further confirmed by high-resolution HAADF-STEM (**Fig. 1C**). The corresponding FFT pattern shows the crystal structure of $PdCd_{0.82}$ NC, where the $PdCd_{0.82}$ NC exposes the (220) crystal face along [001] zone axes (**Fig. 1D**). **Fig. 1E** exhibits enlarged HRTEM image from the area indicated by the white dashed rectangle in **Fig. 1D**. As shown in **Fig. 1F**, the lattice spacing of crystal plane that parallel to the edge of cube is measured to be 0.154 nm, assigning to the (220) plane of PdCd (JCPDS 06-0570). The HAADF-STEM image and corresponding elemental mappings and the line-scan analysis show that Pd and Cd are uniformly distributed throughout the whole NC (**Fig. 1, G, H**).

By simply changing the amount of Cd precursor supplied, with other conditions kept the same as the synthesis of the $PdCd_{0.82}$ NCs, the $PdCd_{0.53}$, $PdCd_{0.67}$ and $PdCd_{1.13}$ NCs were readily obtained (see Materials and Methods). Typical STEM images of the $PdCd_x$ NCs are displayed in **fig. S4, A, D, G,** where all the different $PdCd_x$ NCs exhibit similar morphologies and sizes. Detailed characterizations were further carried out to reveal the crystalline nature and elemental distributions of these $PdCd_x$ NCs. The EDS results show that the atomic ratios of Pd/Cd in $PdCd_{0.53}$, $PdCd_{0.67}$ and $PdCd_{1.13}$ NCs are 64.9/35.1, 60.0/40.0 and 47.2/52.8, respectively, consistent with the ICP-AES results (**fig. S3**). As more Cd is introduced, the PXRD peaks are shifted to smaller 2θ values assigned to the PdCd phase, indicating the increased *d*-spacing and the dilation of the lattice-constant is due to the incorporation of Cd into the Pd *fcc* lattice (**Fig. 2A**). The crystalline nature of these $PdCd_x$ NCs was further characterized by HRTEM (the insets of **fig. S4, A, D, G**). The lattice fringes are all approximately 0.15 nm, which can be assigned to the

(220) plane of PdCd. The spatial distributions of Pd and Cd species in these $PdCd_x$ NCs were then identified by HAADF-STEM, line-scan analysis and elemental mappings, where Pd and Cd are distributed uniformly throughout the NCs (**fig. S4, B, C, E, F, H, I**). Precise surface control of $PdCd_x$ NCs offer a potential for tuning their catalytic properties. X-ray photoelectron spectroscopy (XPS) was carried out to reveal the electronic interaction between the Pd and Cd of $PdCd_x$ NCs (**Fig. 2, B, C**). The $3d_{3/2}$ and $3d_{5/2}$ peaks of Pd in $PdCd_x$ NCs exhibit consecutive negative shifts with increasing Cd, suggesting that there is a slight electron transfer from Cd to Pd. The $3d_{3/2}$ and $3d_{5/2}$ peak positions of Cd in the PdCdx NCs have no obvious shift, but the proportion of metallic Cd peaks are positively correlated with Cd peaks. The *d*-band of $PdCd_x$ NCs further confirmed the electronic interaction between the Pd and Cd, where its center of gravity gradually shifted down with the increasing amounts of Cd (**Fig. 2D**), indicating the variation of adsorption capability for $PdCd_x$ NCs. Therefore, the $PdCd_x$ nanostructures with different compositions exhibit tunable surface properties.

Pd-based nanocatalysts have been widely used in hydrogenation reactions, and the quest for superior hydrogenation nanocatalysts that combine high activity, selectivity, and stability is state-of-the-art research (*25-28*). As a proof-of-concept application, the selective hydrogenation of NPA was first adopted as the model reaction to evaluate the performance of the $PdCd_x$ NCs with different composition ratios. In this study, remarkable selectivity with a switchable feature for all five potential hydrogenation products was successfully realized, and the performance of $PdCd_x$ NCs exhibits an obvious composition dependence as well as a distinct hydrogen source dependence (**Scheme 1**).

In detail, the selective hydrogenation of NPA into NS, 4-Nitroethylbenzene (NEY), 4-Ethylaniline (EA), 4-Aminophenylacetylene (APA) and 4-Aminostyrene (AS) has been readily achieved under optimal hydrogenation conditions (**Fig. 3A**). As a starting point, the $PdCd_{0.82}$ NCs was applied to the hydrogenation of NPA using H_2 as the hydrogen source under mild conditions (see Materials and Methods). As shown in **Fig. 3B**, $PdCd_{0.82}$ NCs exhibits a desirable conversion and selectivity to NS. The main product of NS (97.6 %) and trace NEY (2.4 %) were detected in a very short time period (0.5 h).

The selectivity for NS (96.0 %) was maintained even after a 5 h reaction, indicating that $PdCd_{0.82}$ is only able to reduce alkynyl to vinyl under this reaction condition. Inspired by this result, the hydrogenation properties of $PdCd_{0.53}$, $PdCd_{0.67}$ and $PdCd_{1.13}$ NCs were also tested under identical conditions. For $PdCd_{1.13}$ NCs, the selectivity to NS was still obtained at a suitable level, while the hydrogenation conversion rate was decreased, revealing that an increased Cd content weakens the activity (**fig. S5A**). In contrast, the high conversion rate of NPA still remained for $PdCd_{0.67}$ and $PdCd_{0.53}$ NCs, but the main hydrogenated product was converted to NEY and EA, respectively, indicating that an improved hydrogenation activity can be obtained by decreasing the ratio of Cd (**Fig. 3, C, D**). It is worth noting that the intermediate products of NS and NEY were detected in the initial hydrogenation period over $PdCd_{0.67}$ and $PdCd_{0.53}$ NCs, respectively. Therefore, we can conclude that the product transformation path is from NPA to NEY and eventually to EA under H_2, where the hydrogenation trend of the functional groups is according to the order of alkynyl > vinyl > nitryl under this reaction condition. To confirm this conclusion, we further investigated the hydrogenation properties of these $PdCd_x$ NCs by directly using NS or NEY as the substrate under identical reaction conditions. As shown in **fig. S6A**, the NS is hardly hydrogenated by $PdCd_{1.13}$ and $PdCd_{0.82}$ NCs, while a high conversion could be observed over $PdCd_{0.67}$ and $PdCd_{0.53}$ NCs. As expected, for NEY, only $PdCd_{0.53}$ NCs exhibit a high conversion (**fig. S6B**). Therefore, the satisfied selectivity to the specific products over $PdCd_x$ NCs in NPA hydrogenation mainly results from the activity difference of $PdCd_x$ NCs with different ratios of Cd.

The desired selectivity to NS, NEY and EA has thus been realized, and a distinct composition effect and hydrogenation trend (alkynyl > vinyl > nitryl) have been observed. To further achieve the same level of selectivity to all hydrogenation products, the nitryl must be initially reduced to yield APA and AS. Considering that metal-catalyzed reduction features various reducing agents other than molecular hydrogen (*29-31*), the use of different hydrogen sources might be an efficient approach to change the hydrogenation trend. As a hydrogen source, $HCOONH_4$ is an alternative, simple, and inexpensive reducing agent, which can offer eco-friendly reaction conditions and even enhance efficiency (*30*).

Therefore, we were further motivated to explore the performance of $PdCd_x$ NCs for selective NPA hydrogenation by using $HCOONH_4$. Significantly, a complete switch of selectivity to the products was achieved by changing the hydrogen source from H_2 to $HCOONH_4$. For $PdCd_{1.13}$ NCs, the main hydrogenation product changed from NS to APA under the same hydrogenation conditions by replacing H_2 with $HCOONH_4$ (**Fig. 3E and fig. S5A**). Over the course of the hydrogenation reaction, it is clear that NPA was totally converted after 3 h, and the selectivity of APA reached 92.0 %. AS (8.0 %) was also detected in this process (**Fig. 3E**). The hydrogenation properties of other $PdCd_x$ NCs were also investigated. As shown in **Fig. 3F**, $PdCd_{0.82}$ NCs exhibit a higher hydrogenation conversion rate over $PdCd_{1.13}$ NCs, while the main product is converted to AS (100 %). It is worth noting that the APA was also detected in the initial reaction period, indicating that the hydrogenation reaction proceeded on a different hydrogenation path by changing H_2 with $HCOONH_4$ as the hydrogen source. The $PdCd_{0.67}$ NCs exhibits similar performance to $PdCd_{0.82}$ NCs but are unable to maintain a high selectivity for AS and is further converted to EA after achieving a high conversion level (**fig. S5B**). For the $PdCd_{0.53}$ NCs, it is obvious that all of the NPA was converted into fully hydrogenated EA as the final reduction product (**Fig. 3G**). It is worth emphasizing that the NS and NEY can be detected in short reaction time, indicating the same hydrogenation path over $PdCd_{0.53}$ NCs whether using H_2 or $HCOONH_4$ as the hydrogen source, which demonstrates that the distinct hydrogen source effect can only be observed for the $PdCd_x$ NCs with high Cd contents. Therefore, a distinct hydrogenation path was observed in the NPA hydrogenation by using $HCOONH_4$ as a hydrogen source, where the hydrogenation trend of functional groups is in the order of nitryl > alkynyl > vinyl, in contrast with the hydrogenation reaction by using H_2 as the hydrogen source. In addition, to make a more precise comparison, the turnover frequency (TOF) of $PdCd_x$ NCs based on Pd near the highest selectivity of the desired product was provided. As shown in **Table S3**, the TOF of reactions using H_2 as a hydrogen source is generally higher than that of those using $HCOONH_4$ as a hydrogen source. Meanwhile, the Cd concentration has more effect on the TOF of reactions when using H_2 as the hydrogen source (**Table S3**). Moreover, control experiments of the additional introduction of

NH_3 in the presence of H_2 have been carried out. The results reveal that the hydrogenation rates or products are close to the cases only using H_2 as the hydrogen source (**Fig. S7**), mostly because the excessive supply of H_2 blocks the action of NH_3 and prevents the hydrogenation trend as induced by $HCOOONH_4$. This exactly proves the specific role of $HCOOONH_4$ played in this reaction.

Pd NCs (**fig. S8 and S9**) and $PdCd_{0.82}$ NPs (**fig. S10**) of a similar size were also prepared to better understand the roles of the composition and morphology of $PdCd_x$ NCs in the highly selective hydrogenation reaction. As shown in **fig. S11**, Pd NCs exhibit a much higher hydrogenation rate in the hydrogenation of NPA whether H_2 or $HCOONH_4$ is the hydrogen source, where NPA was fully hydrogenated into EA in a short time. The performance of Pd NCs is very similar to that of the commercial Pd/C (**fig. S12**), demonstrating that the hydrogenation rate is hard to control by pure Pd nanocatalysts and leads to a low selectivity for intermediate products in NPA hydrogenation. These results show that the introduction of Cd to Pd NCs is beneficial for a desirable selectivity for different hydrogenation products of NPA through precisely weakening the activity of Pd. In addition, $PdCd_{0.82}$ NPs were also chosen as references to explore the shape/facet effect in the hydrogenation reaction. As shown in **fig. S13**, $PdCd_{0.82}$ NPs exhibits similar hydrogenation rates but shows a significantly reduced NS or AS selectivity compared with $PdCd_{0.82}$ NCs, whether H_2 or $HCOONH_4$ is the hydrogen source. In other words, the systematic tuning of $PdCd_x$ NCs is essential to achieve the desired competitive level of hydrogenation of NPA into NS, NEY, EA, APA and AS.

To understand the mechanism of two distinct hydrogenation paths over various $PdCd_x$ NCs by using different hydrogen sources, a series of detailed experiments were further carried out. Considering that the surface properties of nanocatalysts largely affect the adsorption/desorption of the substrate and corresponding products, the $PdCd_x$ NCs with different Cd contents can possess different surface properties for the adsorption/desorption of nitryl and alkynyl. To make a direct comparison, experiments involving the hydrogenation of the physical mixture of phenylacetylene (PA) and nitrobenzene (NB) over $PdCd_x$ NCs were conducted under different hydrogen sources. When H_2 is adopted as the hydrogen source, the

hydrogenation rates of PA and NB decrease with the increased content of Cd, but the hydrogenation rate of PA is always much higher than that of NB in all the $PdCd_x$ NC-catalyzed reactions (**fig. S14**). In addition, while $PdCd_{0.82}$ and $PdCd_{1.13}$ NCs maintain a superior selectivity for styrene (SY) at different conversions, $PdCd_{0.53}$ and $PdCd_{0.67}$ NCs struggle to preserve the demanded selectivity for SY as the reaction proceeds. Significantly, a completely different catalytic behavior was observed for all $PdCd_x$ NCs once $HCOONH_4$ was applied as the hydrogen source with other reaction conditions being the same. The hydrogenation rate of PA by using $HCOONH_4$ as the hydrogen source is slightly lower than that of H_2, while a much higher hydrogenation rate of NB was obtained, which is even higher than the hydrogenation rate of PA (**fig. S15**). The contrary results of the hydrogenation rates for PA and NB with different hydrogen sources are consistent with the different selectivity of NPA hydrogenation by using different hydrogen sources.

To illuminate the influence of the surfaces of $PdCd_x$ NCs with different compositions on the catalytic performance, we used density functional theory (DFT) to investigate the catalytic processes. First, we constructed PdCd NCs with a (220) surface that matched with the experimental results. To simulate different compositions, we built the surface for pure Pd and $PdCd_x$ NCs with ratios of Pd to Cd as 0.5, 0.8 and 1.25, respectively, on the top surface of the (220) plane (**fig. S16**). As shown in **table S1**, the electron transferred from Cd to Pd increases when the concentration of Cd increases and the trend matches well with XPS results. We further performed adsorption energy analysis for these established models. Since $HCOONH_4$ decomposes to HCOOH and NH_3, the HCOOH is the main reductive part as the hydrogen source in our simulations. As shown in **tables S2 and S4**, the adsorption of all the species (including the substrate, hydrogen sources, and possible products) decreases as the Cd concentration increases. Strong adsorption of the substrate and hydrogen sources implies high catalytic efficiency. Therefore, the activity of the $PdCd_x$ NCs decreases with higher Cd concentrations.

The distinct hydrogen source (H_2 or $HCOONH_4$) dependence for $PdCd_x$ NCs in hydrogenation reactions is also considered in this simulation. H_2 should be adsorbed on the metal surface first and then

be activated to hydrogenate the substrates. **Fig. 4A** shows the optimized configurations of NPA, NS and NEY adsorbed on the surface of pure Pd and $PdCd_x$ NCs. Notably, Pd or Cd is in the coordinated environment that displays stronger bindings with alkynyl and vinyl groups than nitryl groups on the surface of Pd and $PdCd_x$ NCs, so that alkynyl and vinyl groups would be hydrogenated preferentially, which is in agreement with the reductive order (alkynyl > vinyl > nitryl) observed experimentally. $HCOONH_4$ can be ionized into $HCOO^-$, NH_3 and H^+ in solutions (**Equation 1**). $HCOO^-$ can provide a negatively charged H^- anion (**Equation 2**) that is highly reductive and nucleophilic, where the H^- anion prefers to attack N atoms with positive charges in nitryl groups; when the reduction reaction starts, the proton H^+ would attack the O atom with a negative charge in a nitryl group (**fig. S17**). On the other hand, $HCOO^-$ and H^+ would be adsorbed on the metal surface as hydrogen donors and then react with the adsorbed alkynyl and vinyl groups. Therefore, the reduction of nitryl groups has an E-R (Eley-Rideal) mechanism, and the hydrogenation of alkynyl and vinyl groups has a L-H (Langmuir-Hinshelwood) mechanism when $HCOONH_4$ is used as the hydrogen source (*32*). The reduction of nitryl groups will occur more preferentially than the hydrogenation of alkynyl and vinyl groups because it directly reacts with $HCOO^-$ (or H^+) without the need for $HCOO^-$ (or H^+) to be adsorbed on the metal surface and the transfer of H to the surface.

Whether H_2 or $HCOONH_4$ is used as a source of hydrogen, the selectivity has been tuned with the increase of Cd concentration. As shown in **Fig. 4**, **B**, **C**, we studied the mechanisms of hydrogenation of phenylacetylene to phenylethane on the $PdCd_{0.5}$ (220) surface and $PdCd_{1.25}$ (220) surface by the transition state (TS) search and the related structures can be seen in **fig. S18**. It is noticed that on the $PdCd_{0.5}$(220) surface, the adsorption energies of phenylacetylene and styrene are -1.74 eV and -1.20 eV, respectively, which are much larger than the activation barriers, thus leading to the final product being phenylethane. However, on the $PdCd_{1.25}$(220) surface, the activated barriers of the first and third reaction steps reach 1.18 eV and 1.90 eV, which are much higher than the adsorption energies of phenylacetylene and styrene. These data indicate that on the $PdCd_{1.25}$ (220) surface, it is not easy for the reaction to occur and the

catalytic activity is low. When the concentration of Cd doping increases, on the one hand, the adsorption of reactants (phenylacetylene, styrene) has weakening effects, on the other hand, the activation barriers of reactions on $PdCd_{1.25}$ surfaces are higher than that on $PdCd_{0.5}$ surfaces. Both results show that $PdCd_{1.25}$ is less effective than $PdCd_{0.5}$ for the reaction of the hydrogenation of phenylacetylene to occur. This is consistent with the phenomena observed in the experiment: the increase of Cd concentration weakens the catalytic effect on the hydrogenation of phenylacetylene. Therefore, the adsorption energies of the substrates are significantly reduced as the Cd concentration increases. That is, the decreases of the adsorption energies can protect intermediates from further hydrogenation and lead to the final product since it will be more easily desorbed from the surface. Based on this rule, we could determine the final product in different situations. For example, for $PdCd_{0.5}$ with H_2 as the hydrogen source, EA will be the final product because its adsorption energy of -1.32 eV is lower than that of NS and NEY. For $PdCd_{0.8}$, the adsorption configuration shows that NEY is parallel to the surface and does not bind to the metal surface, indicating the physical adsorption of NEY on the $PdCd_{0.8}$ surface rather than the chemical bindings. Additionally, NEY has the minimum adsorption energy of -0.98 eV (**table S4**); thus, NEY would desorb most easily and become the final product. The case of PdCd has a similar trend to that of $PdCd_{0.8}$. Finally, NS will be the final product on the $PdCd_{1.25}$ surface due to its lowest adsorption energy of -0.87 eV. This trend is fully in line with the experimental data. When $HCOONH_4$ is the hydrogen source, in which case EA, AS, and APA are the possible products, we could also determine the final product based on the minimum adsorption energy rule from **table S4**, and the trend is also consistent with the experimental data. Furthermore, the differences between the adsorption energies of NPA and NS (NS and NEY, APA and AS, AS and EA) decrease with increasing Cd concentrations, indicating that the adsorption energy of the reactants and the corresponding reduction products are getting closer. Thus, the reactant tends to be desorbed more easily, broadly agreeing with the experimental results.

Encouraged by these efficient hydrogenation results, hydrogenation reactions with other similar substrates (NBAD and NS) over $PdCd_x$ NCs were also carried out. As expected, a desirable level of

conversion for NBAD and a competitive NS selectivity for all potential hydrogenation products have been achieved under the optimized hydrogenation conditions (**table S5 and table S6**), which also exhibits an obvious composition dependence and a distinct hydrogen source dependence. From the comparison of catalysts performance in our work with some benchmark catalysts in others' works, it is apparent that most previous studies solely focused on achieving a high selectivity of one desired hydrogenated product. In contrast, the realization of high selectivity for all potential hydrogenation products under one catalysis system is the most striking feature of our work (**Table S3**).

A practically relevant hydrogenation catalyst should exhibit both high performance (activity and selectivity) and excellent stability. We have also evaluated the stability of $PdCd_x$ NCs by consecutive reactions, where constant amounts of substrate were added in each run. As shown in **Fig. 5 and fig. S19**, after being reused six times, a superior conversion level was maintained for all $PdCd_x$ NCs, with no obvious deactivation of the $PdCd_x$ NCs in the consecutive reactions. Significantly, a competative selectivity to different hydrogenation products of NPA was largely maintained, confirming that the hydrogenation properties of these $PdCd_x$ NCs were almost unchanged. The detailed characterizations for the catalysts after recycling experiments were carried out. It is clear to see that there are no obvious morphology/composition changes after hydrogenation in these cases (**fig. S20**). Uniform elemental distributions have been also confirmed by the elemental mappings and the line-scan analysis (**fig. S21**). Further XPS studies reveal that there are no obvious differences of Pd and Cd for catalysts after hydrogenations by using two different hydrogen sources, indicating a similar surface structure in both cases after catalysis **(fig. S22**). Therefore, we can conclude that a different reaction selectivity should be caused by different hydrogen sources but not from the surface structure alteration.

In summary, we have presented a wet-chemical strategy for a series of well-defined and uniform nanocubic $PdCd_x$ nanocatalysts with a tunable composition for the flexible selectivity control of NPA hydrogenation for all potential hydrogenation products. The performance of the $PdCd_x$ NCs exhibited strong dependence of both composition tuning and hydrogen sources selections, , where the irreplaceable

role of Cd and uniform nanocube morphology in the remarkable selective hydrogenation has been identified. DFT calculations have been performed to elucidate the origin underlying the exceptional selectivity of $PdCd_x$ NCs, in which the tuning of adsorption energy of hydrogenation products by precise modulation of Cd play a key role in boosting the selectivity. The $PdCd_x$ NCs also exhibit excellent reusability with negligible activity/selectivity decay and structure/composition changes after consecutive reactions. The generality of the outstanding hydrogenation performance of $PdCd_x$ can be readily applied to other similar substrates (e.g., NBAD and NS). The present finding opens promising opportunities towards the rational design of practically relevant hydrogenation nanocatalysts with extremely high selectivity for broad applications such as fine chemical production and beyond.

MATERIALS AND METHODS

Chemicals. Bis(acetylacetonate)palladium(II) ($Pd(acac)_2$, 99%), sodium tetrachloropalladate(II) (Na_2PdCl_4, > 98%), oleylamine ($C_{18}H_{37}N$, OAm, > 70%), oleic acid ($C_{18}H_{34}O_2$, OA, > 85%), polyvinylpyrrolidone (PVP, K30) and commercial Pd/C (10 wt%, 2-5 nm Pd nanoparticles) were all purchased from Sigma-Aldrich. Cadmium acetate dihydrate ($Cd(CH_3COO)_2 \cdot 2H_2O$, $CdAc_2 \cdot 2H_2O$ > 99.99%) and ricinoleic acid ($C_{18}H_{34}O_3$, RA, > 97%) were purchased from Aladdin. DL-mandelic acid ($C_8H_8O_3$, > 99%) was purchased from Energy Chemical. Benzoin ($C_{14}H_{12}O_2$, > 98%) was purchased from Acros. 4-Nitrophenylacetylene ($C_8H_2NO_2$, NPA, > 99%) was purchased from Beijing HWARK Chem. Cyclohexane (C_6H_{12}, analytical reagent, ⩾ 99.5%), ethanol (C_2H_6O, analytical reagent, ⩾ 99.7%), N, N-Dimethylformamide (DMF, ⩾ 99.5%), formic acid (CH_2O_2, analytical reagent, ⩾ 99.9%), acetone (C_3H_6O, ⩾ 99.9%) and sodium iodide (NaI, analytical reagent, ⩾ 99.9%) were all purchased from Sinopharm Chemical Reagent Co. Ltd. (Shanghai, China). All the chemicals were used as received without further purification. The water (18 MΩ cm^{-1}) used in all experiments was obtained by passing through an ultra-pure purification system (Aqua Solutions).

Synthesis of $PdCd_x$ NCs and $PdCd_{0.82}$ NPs. In a typical preparation of $PdCd_{0.82}$ NCs, $Pd(acac)_2$ (7.6 mg), $CdAc_2 \cdot 2H_2O$ (8.8 mg), DL-mandelic acid (150.0 mg), OAm (4 mL) and OA (1 mL) were added to a vial (volume: 30 mL). After the vial had been capped, the mixture was ultrasonicated for approximately 0.5 h. The resulting homogeneous mixture was heated from room temperature to 160 °C for approximately 0.5 h and kept at 160 °C for 5 h in an oil bath. After cooling to room temperature, the colloidal products were collected by centrifugation and washed with a cyclohexane/ethanol mixture. For the syntheses of $PdCd_{0.53}$, $PdCd_{0.67}$, and $PdCd_{1.13}$ NCs, all the conditions are similar to those of $PdCd_{0.82}$ NCs, except for changing the amount of $CdAc_2 \cdot 2H_2O$ to 4.4 mg, 6.6 mg, and 11.0 mg, respectively. The preparation of $PdCd_{0.82}$ NPs is similar to that of $PdCd_{0.82}$ NCs, except for replacing DL-mandelic acid (150.0 mg) with benzoin (150.0 mg).

Synthesis of Pd NCs. In a typical preparation of Pd NCs, Na_2PdCl_4 (7.4 mg), PVP (100 mg), NaI (5 mg), and DMF (10 mL) were added to a vial (volume: 30 mL). After the vial had been capped, the mixture was ultrasonicated for approximately 10 min. The resulting homogeneous mixture was heated from room temperature to 120 °C for approximately 0.5 h and kept at 120 °C for 5 h in an oil bath. After cooling to room temperature, the colloidal products were collected by centrifugation and washed with an ethanol/acetone mixture three times.

Characterization. The samples were prepared for characterization by dropping their cyclohexane or ethanol dispersions onto carbon-coated copper grids using pipettes. The grids were dried under ambient conditions. Low-magnification TEM was conducted on a HITACHI HT7700 transmission electron microscope at an acceleration voltage of 120 kV. High-magnification TEM and STEM were conducted on an FEI Tecnai F20 transmission electron microscope at an acceleration voltage of 200 kV. PXRD patterns were collected on X'Pert-Pro MPD diffractometer (Netherlands PANalytical) with a Cu Kα X-ray source (λ = 1.540598 Å). The concentration of catalyst was determined by ICP-AES (Varian 710-ES). All the X-ray photoelectron spectroscopy (XPS) measurements of these catalysts were collected with a Thermo Scientific, ESCALAB 250 XI system.

Hydrogenation measurements. The obtained $PdCd_x$ NCs, $PdCd_{0.82}$ NPs and Pd NCs were further loaded on carbon black (Vulcan XC72R carbon, C) with a total Pd content of 5 wt%, as determined by ICP-AES. All the hydrogenation runs were performed in a glass pressure vessel (volume: 48 mL, Chemical glass), to which solvent (10 mL, DMF), $PdCd_x$ (x = 0.53, 0.67, 0.82, 1.13) (10 mg, 5 wt%) and substrate (0.68 mmol NPA/NBAD/NS) were added. When H_2 was the hydrogen source, the glass pressure vessel was sealed and purged three times with H_2 under stirring. The glass pressure vessel was then pressurized to 0.1 MPa using H_2 and heated to 60 °C under constant stirring. When $HCOONH_4$ was the hydrogen source, $HCOONH_4$ (1.5 mmol) was added to the glass pressure vessel. The glass pressure vessel was then sealed and heated to 60 °C under constant stirring. Samples were taken at fixed intervals by a sample tube. The samples were filtered and analyzed by a gas chromatograph (GC, Shanghai Yiyou, GC-7860, column: HP-5, 30 m × 0.32 mm × 0.25 μm) with a flame ionization detector (FID). All hydrogenation runs of $PdCd_{0.82}$ NPs, Pd NCs and the commercial Pd/C were performed under the same conditions, changing $PdCd_x$ NCs to $PdCd_{0.82}$ NPs, Pd NCs and the commercial Pd/C. The turnover frequency numbers (TOF) based on Pd of these catalysts was calculated using the following equation.

$$\mathrm{TOF}(h^{-1}) = \frac{n_{substrate}(mmol) \times \mathrm{Conversion}}{n_{Pd}(mmol) \times t(h)} = \frac{n_{substrate}(mmol) \times \mathrm{Conversion}}{\frac{m_{cat}(g) \times \mathrm{Pd}\ wt\ \%}{M_{Pd} \times 10^{-3}(g\ mmol^{-1})} \times t(h)}$$

DFT models and calculations. All the calculations were performed with the "Vienna ab initio simulation package" (VASP5.4.4) (*33-36*). The electron interactions were represented by the projector augmented wave (PAW) method and plane-wave basis functions with a kinetic energy cut-off of 400 eV (*37*). The electronic interaction effect in the calculations was described by the generalized gradient approximation (GGA) with the Perdew-Burke-Ernzerh (PBE) functional. Ground-state atomic geometries were obtained by minimizing the energy and force to 1.0×10^{-5} eV/atom and 0.05 eV/Å, respectively. To examine the effect of van der Waals interactions on reaction energetics, calculations were performed by using the DFT-D3 functional (*38*). The vacuum spacing in the direction along the Z axis, with respect to the surface, was

15 Å between neighboring slab images, which is sufficient to eliminate the interactions between the slabs. The climbing image nudged elastic band (CI-NEB) method was used to search the transition states and track minimum-energy paths for the reactions (*39-40*).

The optimized lattice parameters for the primitive PdCd are 3.06, 3.06 and 3.76 Å. The PdCd [220] surface was modeled by a 3x3 supercell. All the slabs contained four atomic layers, and the top two layers were allowed to relax. For the calculation of the adsorption energy of small molecules on the slabs, we provide a definition for the calculation of the adsorption energy (E_{ad}) as:

$$E_{ad} = E_{slab\&mol} - (E_{mol} + E_{slab})$$

where $E_{slab\&mol}$, E_{mol}, and E_{slab} are the energies of the slabs with the adsorbed molecule, the single molecule and the slabs, respectively.

SUPPLEMENTARY MATERIALS

Fig. S1. TEM images of PdCd nanostructures prepared under the same condition of $PdCd_{0.82}$ NCs but varying the amounts of OA.

Fig. S2. TEM images of PdCd nanostructures prepared under the same condition of PdCd0.82 NCs but varying the amounts of DL-mandelic acid

Fig. S3. EDS and ICP-AES results of different $PdCd_x$ NCs.

Fig. S4. HAADF-STEM images, line-scan analysis and elemental mappings of $PdCd_{0.53}$ NCs, $PdCd_{0.67}$ NCs and $PdCd_{1.13}$ NCs.

Fig. S5. The conversion of NPA and selectivity vs. time using H_2 and $HCOONH_4$ as hydrogen source over $PdCd_{1.13}$ NCs and $PdCd_{0.67}$ NCs, respectively.

Fig. S6. The conversion of NS and NEY vs. time using H_2 as hydrogen source over different $PdCd_x$ NCs.

REFERENCES AND NOTES

1. D. Wang, Q. Chen, S. Lu, Y. Zhou, Asymmetric hydrogenation of heteroarenes and arenes. *Chem. Rev.* **112**, 2557-2590 (2012).
2. F. Meemken, A. Baiker, Recent progress in heterogeneous asymmetric hydrogenation of C=O and C=C bonds on supported noble metal catalysts. *Chem. Rev.* **117**, 11522-11569 (2017).
3. A. Corma, P. Serna, Chemoselective hydrogenation of nitro compounds with supported gold catalysts. *Science* **313**, 332-334 (2006).
4. B. Wu, H. Huang, J. Yang, N. Zheng, G. Fu, Selective hydrogenation of α, β-unsaturated aldehydes catalyzed by amine-capped platinum-cobalt nanocrystals. *Angew. Chem. Int. Ed.* **124**, 3496-3499 (2012).
5. G. Chen *et al.* Interfacial electronic effects control the reaction selectivity of platinum catalysts. *Nat. Mater.* **15**, 564-569 (2016).

6. S. T. Marshall et al. Controlled selectivity for palladium catalysts using self-assembled monolayers. *Nat. Mater.* **9**, 853-858 (2010).

7. J. G. Ulan, E. Kuo, W. F. Maier, R. S. Rai, G. Thomas, Effect of lead acetate in the preparation of the Lindlar catalyst. *J. Org. Chem.* **52**, 3126-3132 (1987).

8. X. Wang, D. Liu, S. Song, H. Zhang, Pt@CeO_2 multicore@shell self-assembled nanospheres: clean synthesis, structure optimization, and catalytic applications. *J. Am. Chem. Soc.* **135**, 15864-15872 (2013).

9. S. Song *et al.* Achieving the trade-off between selectivity and activity in semihydrogenation of alkynes by fabrication of (asymmetrical Pd@Ag Core)@(CeO_2 Shell) nanocatalysts via autoredox reaction. *Adv. Mater.* **29**, 1605332-1605338 (2017).

10. H. Tian *et al.* The development of yolk-Shell-Structured Pd&ZnO@carbon submicroreactors with high selectivity and stability. *Adv. Funct. Mater.* 1801737 (2018).

11. P. Liu, R. Qin, G. Fu, N. Zheng, Surface coordination chemistry of metal nanomaterials. *J. Am. Chem. Soc.* **139**, 2122-2131 (2017).

12. M. Li *et al.* PdPt alloy nanocatalysts supported on TiO_2: maneuvering metal-hydrogen interactions for light-driven and water-donating selective alkyne semihydrogenation. *Small* **13**, 1604173-1604173 (2017).

13. C. W. A. Chan *et al.* Interstitial modification of palladium nanoparticles with boron atoms as a green catalyst for selective hydrogenation. *Nat. Commun.* **5**, 5787 (2014).

14. W. Niu, Y. Gao, W. Zhang, N. Yan, X. Lu, Pd-Pb alloy nanocrystals with tailored composition for semihydrogenation: taking advantage of catalyst poisoning. *Angew. Chem. Int. Ed.* **127**, 8389-8392 (2015).

15. H. Wei *et al.* FeO_x-supported platinum single-atom and pseudo-single-atom catalysts for chemoselective hydrogenation of functionalized nitroarenes. *Nat. Commun.* **5**, 5634 (2014).

16. T. Mitsudome, M. Yamamoto, Z. Maeno, T. Mizugaki, K. Jitsukawa, One-step synthesis of core-Gold/shell-Ceria nanomaterial and its catalysis for highly selective semihydrogenation of alkynes. *J. Am. Chem. Soc.* **137**, 13452-13455 (2015).

17. K. R. Kahsar, D. K. Schwartz, J. W. Medlin, Control of metal catalyst selectivity through specific noncovalent molecular interactions. *J. Am. Chem. Soc.* **136**, 520-526 (2014).

18. M. Zhao *et al.* Metal-organic frameworks as selectivity regulators for hydrogenation reactions. *Nature* **539**, 76-80 (2016).

19. Gallezot, P. Conversion of biomass to selected chemical products. *Chem. Soc. Rev.* **41**, 1538-1558 (2012).

20. Y. Cao, Z. Sui, Y. Zhu, X. Zhou, D. Chen, Selective hydrogenation of acetylene over Pd-In/Al_2O_3 catalyst: promotional effect of indium and composition-dependent performance. *ACS Catal.* **7**, 7835-7846 (2017).

21. Z. Zhang, B. Xu, X. Wang, Engineering nanointerfaces for nanocatalysis. *Chem. Soc. Rev.* **43**, 7870-7876 (2014).

22. S. Schauermann, N. Nilius, S. Shaikhutdinov, H. Freund, Nanoparticles for heterogeneous catalysis: new mechanistic insights. *Acc. Chem. Res.* **46** 1673-1681 (2012).

23. L. Shao *et al.* Nanosizing intermetallic compounds onto carbon nanotubes: activeand selective hydrogenation catalysts. *Angew. Chem. Int. Ed.* **50**, 10231-10235 (2011).

24. I. Lee, F. Delbecq, R. Morales, M. A. Albiter, F. Zaera, Tuning selectivity in catalysis by controlling particle shape. *Nat. Mater.* **8**, 132 (2009).

25. J. Gu, Y. W. Zhang, F. F. Tao, Shape control of bimetallic nanocatalysts through well-designed colloidal chemistry approaches. *Chem. Soc. Rev.* **41**, 8050-8065 (2012).

26. G. Pei *et al.* Ag alloyed Pd single-atom catalysts for efficient selective hydrogenation of acetylene to ethylene in excess ethylene. *ACS Catal.* **5**, 3717-3725 (2015).

27. C. Oger, L. Balas, T. Durand, J. M. Galano, Are alkyne reductions chemo-, regio-, and stereoselective enough to provide pure (Z)-olefins in polyfunctionalized bioactive molecules? *Chem. Rev.* **113**, 1313-1350 (2013).

28. J. Qi *et al.* Multi-shelled hollow micro-/nanostructures. *Chem. Soc. Rev.* **44**, 6749-6773 (2015).

29. C. H. Zhu *et al.* Visible-light-driven selective photocatalytic hydrogenation of cinnamaldehyde over Au/SiC catalysts. *J. Am. Chem. Soc.* **138**, 9361-9364 (2016).

30. C. Zhu, K. Saito, M. Yamanaka, T. Akiyama, Benzothiazoline: Versatile hydrogen donor for organocatalytic transfer hydrogenation. *Acc. Chem. Res.* **48**, 388-398 (2015).

31. L. He *et al.* Efficient and selective room-temperature gold-catalyzed reduction of nitro compounds with CO and H_2O as the hydrogen source. *Angew. Chem. Inter. Ed.* **48**, 9538-9541 (2009).

32. E. W. Kuipers, A. Vardi, A. Danon, A. Amirav, Surface-Molecule Proton Transfer: A Demonstration of the Eley-Rideal Mechanism *Phys. Rev. Lett.* **66**, 116-119 (1991).

33. G. Kresse, D. Joubert, From ultrasoft pseudopotentials to the projector augmented-wave method. *Phys. Rev. B.* **59**, 1758-1775 (1999).

34. G. Kresse, J. Furthmuller, Efficient iterative schemes for ab initio total-energy calculations using a plane-wave basis set. *Phys. Rev. B.* **54**, 11169-11186 (1996).

35. P. E. Blochl, Projector augmented-wave method. *Phys. Rev. B.* **50**, 17953-17979 (1994).

36. G. Kresse, J. Hafner, Ab-initio molecular-dynamics simulation of the liquid-metal amorphous-semiconductor transition in germanium. *Phys. Rev. B.* **49**, 14251-14269 (1994).

37. J. P. Perdew, K. Burke, M. Ernzerhof, Generalized gradient approximation made simple. *Phys, Rev. Lett.* **77**, 3865-3868 (1996).

38. S. Grimme, J. Antony, S. Ehrlich, H. Krieg, A consistent and accurate ab initio parametrization of density functional dispersion correction (DFT-D) for the 94 elements H-Pu. *J. Chem. Phys.* **132**, 154104 (2010).

39. G. Henkelman, B. P. Uberuaga, H. Jonsson, A climbing image nudged elastic band method for finding saddle points and minimum energy paths. *J. Chem. Phys.* **113**, 9901-9904 (2000).

40. G. Mills, H. Jonsson, G. K. Schenter, Reversible work transition-state theory-application to dissociative adsorption of hydrogen. *Surf. Sci.* **324**, 305-337 (1995).

41. M. Tejeda-Serrano *et al*. Synthesis of supported planar iron oxide nanoparticles and their chemo- and stereoselectivity for hydrogenation of alkynes. *ACS. Catal.* **7**, 3721-3729 (2017).

42. J. Mao et al. Rational Control on the Selectivity of Ru Catalyst for Hydrogenation of 4-Nitrostyrene via Strain Regulation. *Angew. Chem.* **129**, 12133-12137 (2017).

43. N. Yang *et al.* Amorphous/crystalline hetero-phase Pd nanosheets: one-pot synthesis and highly selective hydrogenation reaction. *Adv. Mater.* **30**, 1803234 (2018).

44. M. Makosch *et al.* Organic thiol modified Pt/TiO_2 catalysts to control chemoselective hydrogenation of substituted nitroarenes. *ACS Catal.* **2**, 2079-2081 (2012).

45. M. J. Beier *et al.* Tuning the chemoselective hydrogenation of nitrostyrenes catalyzed by ionic liquid-supported platinum nanoparticles. *ACS Catal.* **2**, 2587-2595 (2012).

46. S. Cai *et al*. Highly active and selective catalysis of bimetallic Rh_3Ni_1 nanoparticles in the hydrogenation of nitroarenes. *ACS Catal.* **3**, 608-612 (2013).

ACKNOWLEDGEMENTS

Fundings: This work was financially supported by the Ministry of Science and Technology (2016YFA0204100, 2017YFA0208200), the National Natural Science Foundation of China (21571135), Young Thousand Talented Program, Six Talent Peak Project in Jiangsu Province (Grant No. XNY-042), the Collaborative Innovation Center of Suzhou Nano Science & Technology, the Priority Academic Program Development of Jiangsu Higher Education Institutions (PAPD), the 111 Project, and Joint International Research Laboratory of Carbon-Based Functional Materials and Devices, and the start-up supports from Soochow University.

Author contributions: X.H. conceived and supervised the research. X.H., Y.F. and Q.S. designed the experiments. X.H., Y.F., Q.S., S.B. and S.Y. performed most of the experiments and data analysis. X.H., Y.F., Q.S. and X.Z. participated in various aspects of the experiments and discussions. L.X., B.H. and W.X. performed the DFT simulations. X.H. and Y.F. wrote the paper. All authors discussed the results and commented on the manuscript.

Competing interests: The authors declare that there are no competing financial interests.

Data and materials availability: All data needed to evaluate the conclusions in the paper are present in the paper and/or the Supplementary Materials. Additional data related to this paper may be requested from the authors.

FIGURES AND LEGENDS

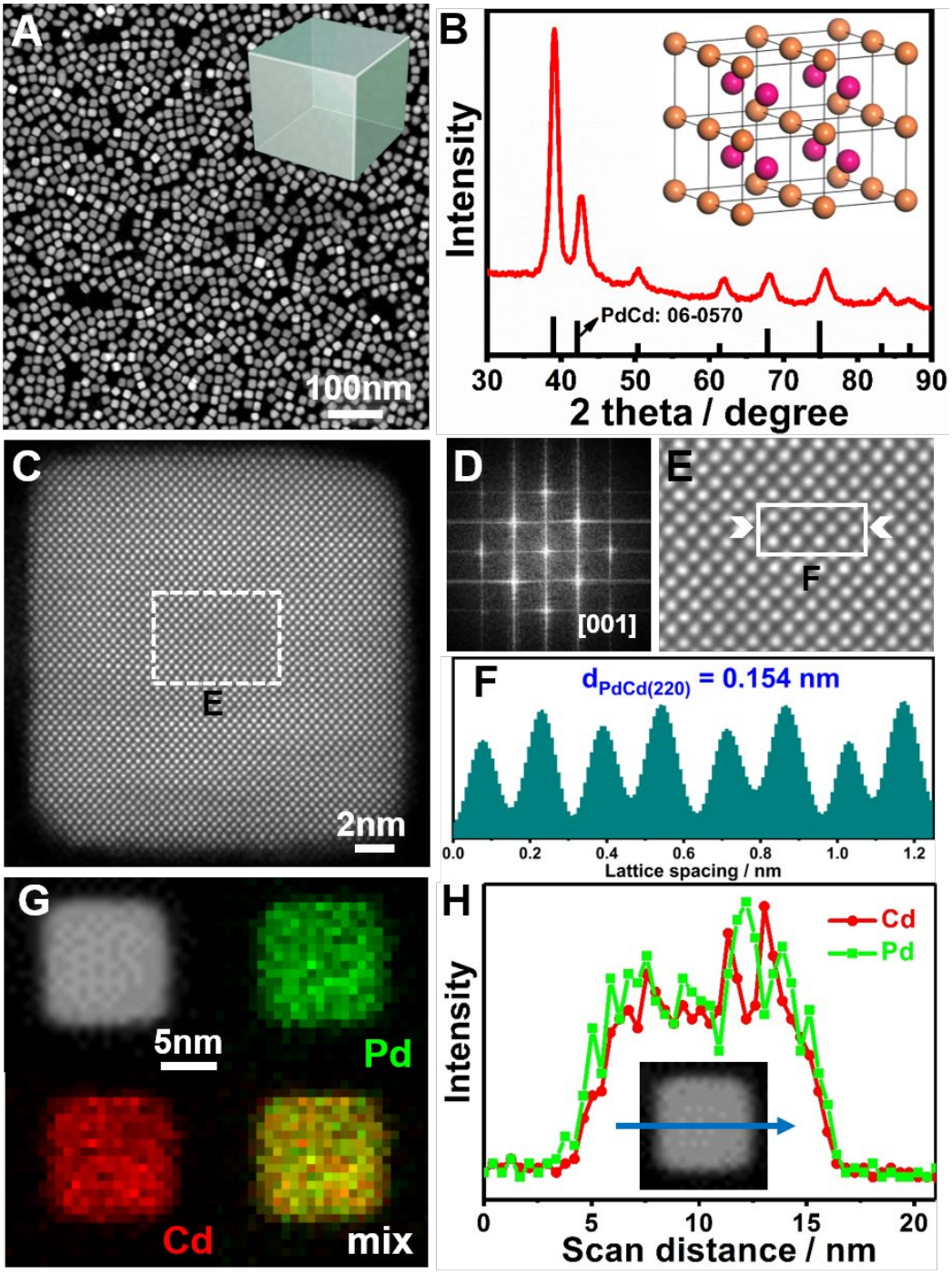

Fig. 1 Morphological and Structural Characterizations of $PdCd_{0.82}$ NCs. (**A**) HAADF-STEM image and (**B**) PXRD pattern of $PdCd_{0.82}$ NCs. (**C**) High resolution HAADF-STEM image of $PdCd_{0.82}$ NC. (**D**) Corresponding FFT image of (**C**). (**E**) Enlarged high resolution HAADF-STEM image from the selected area in (**C**). (**F**) Integrated pixel intensities of PdCd (taken from the white solid rectangle in (**E**)) along the arrow directions, which are perpendicular to the (220) facet. (**G**) HAADF-STEM image and corresponding

elemental mappings and (**H**) line-scan analysis across the blue arrow. Inset in (A), cube model of Pd-Cd. Inset in (**B**), atomic model of Pd-Cd.

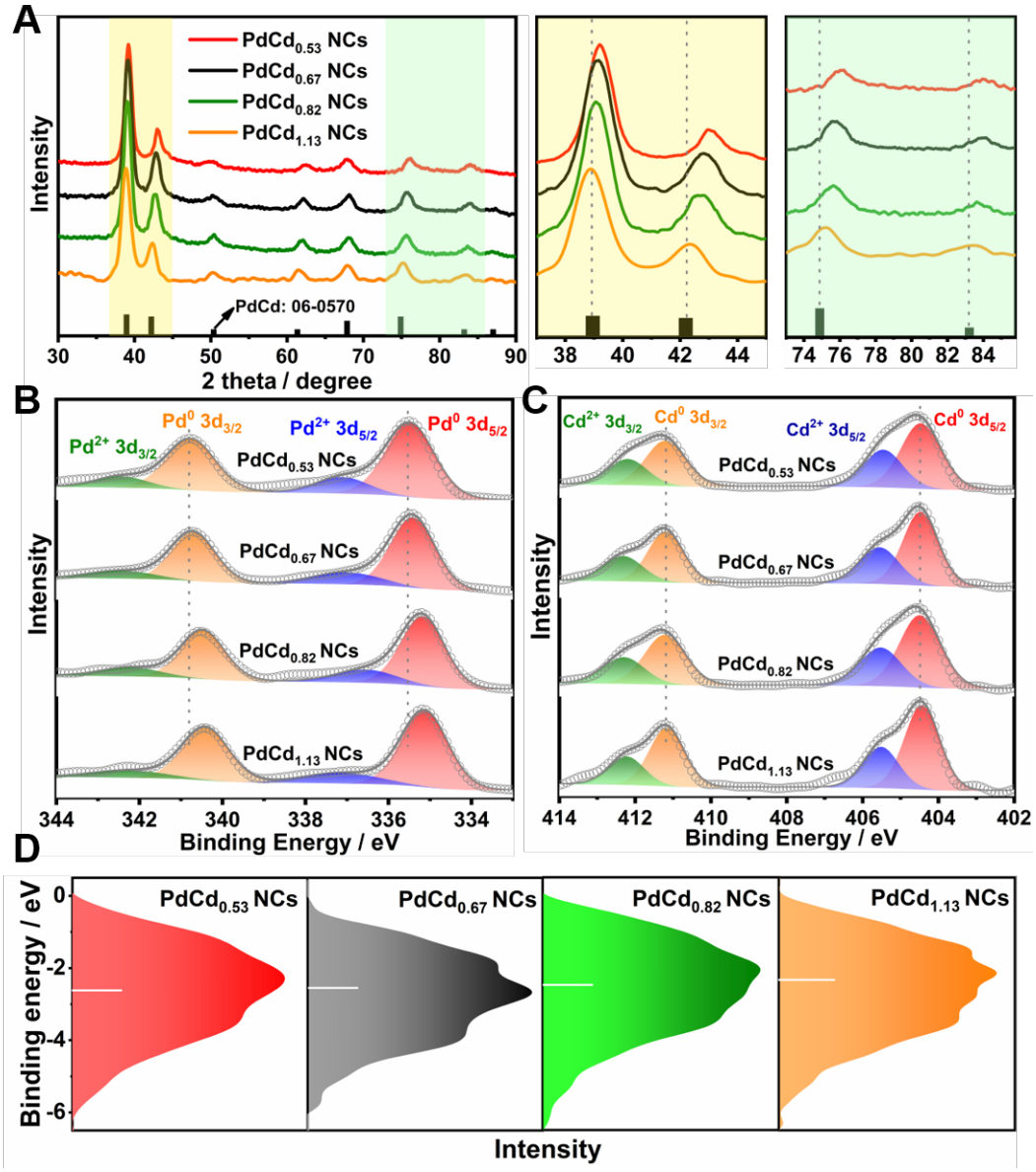

Fig. 2 Structural Characterizations of $PdCd_x$ NCs. (**A**) PXRD patterns and enlarged PXRD patterns of $PdCd_x$ NCs. XPS spectra of (**B**) Pd 3*d* and (**C**) Cd 3*d* of different $PdCd_x$ NCs. (**D**) Surface valence band of $PdCd_x$ NCs. All the spectra are background corrected. The white bar indicates the center of gravity.

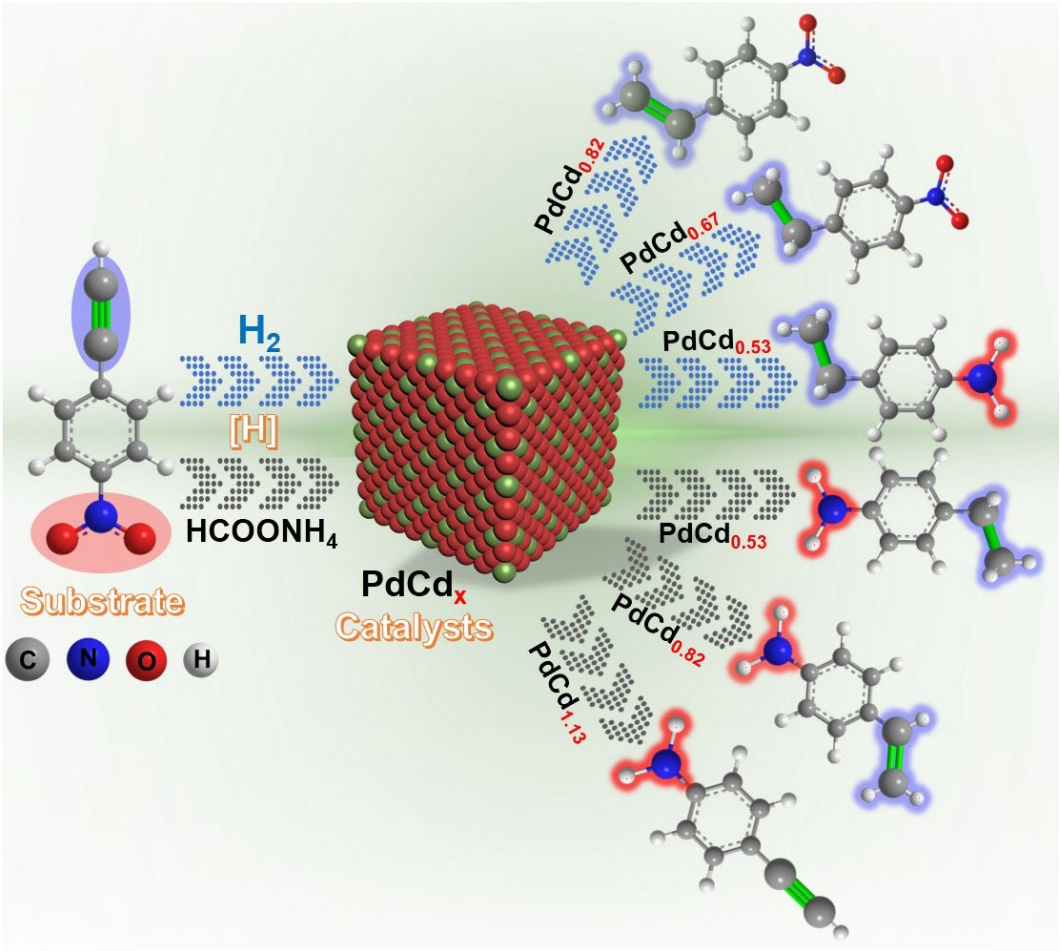

Scheme 1. Schematic illustration showing two distinct hydrogenation paths over $PdCd_x$ NCs using H_2 and $HCOONH_4$ as hydrogen sources.

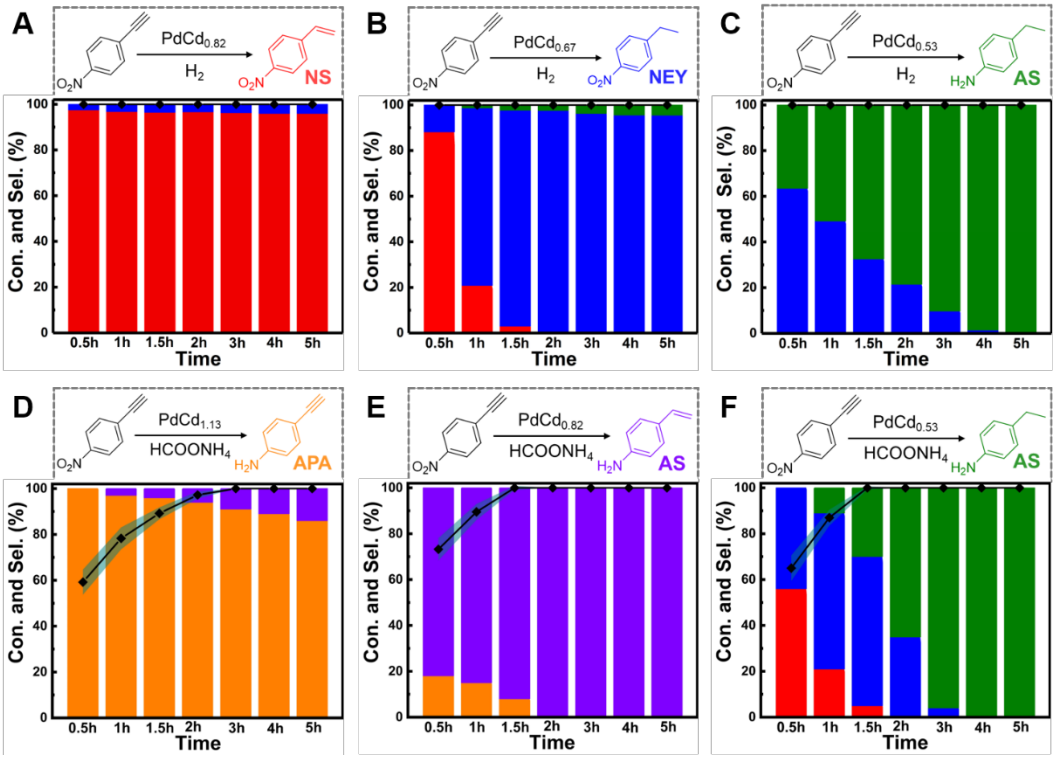

Fig. 3 Hydrogenation of NPA over $PdCd_x$ NCs. The conversion of NPA and selectivity to specific products vs. time using H_2 as the hydrogen source over (**A**) $PdCd_{0.82}$ NCs, (**B**) $PdCd_{0.67}$ NCs and (**C**) $PdCd_{0.53}$ NCs. The conversion of NPA and selectivity to specific products vs. time using $HCOONH_4$ as the hydrogen source over (**D**) $PdCd_{1.13}$ NCs, (**E**) $PdCd_{0.82}$ NCs and (**F**) $PdCd_{0.53}$ NCs. The light blue areas in (**D, E, F**) represent error bars of conversion.

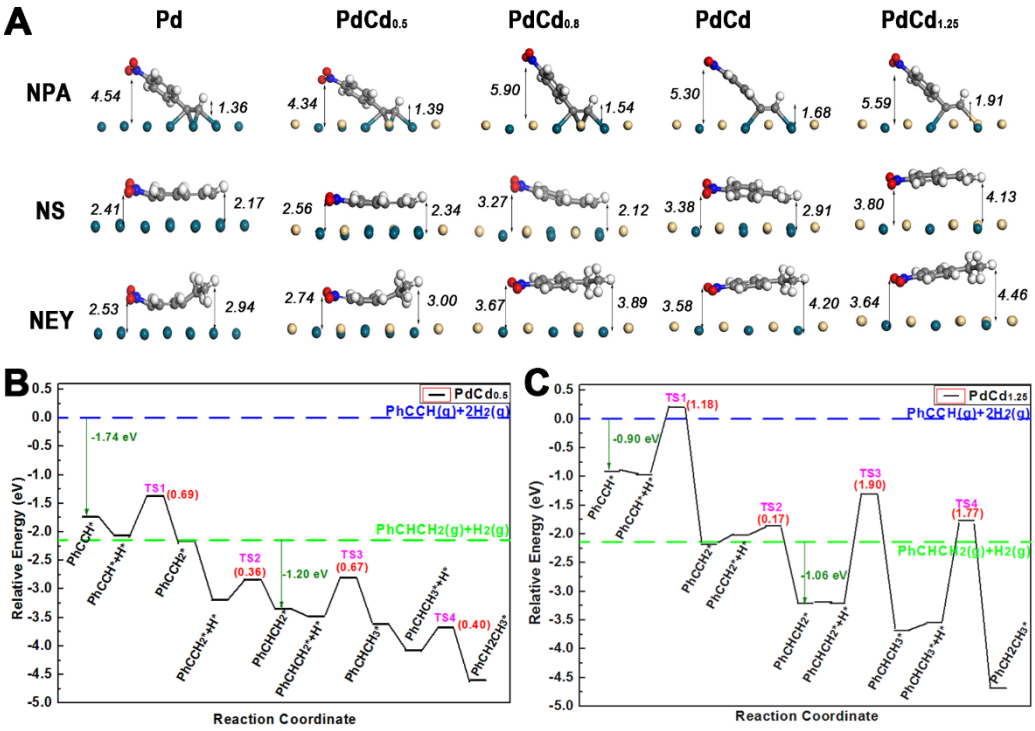

Fig. 4 The adsorption configurations of adsorbates on pure Pd and $PdCd_x$ NCs and reaction pathway for the hydrogenation of phenylacetylene on the $PdCd_{0.5}$ (220) surface. (**A**) The different optimized configurations of NPA, NS and NEY adsorbed on the surface of pure Pd and $PdCd_x$ NCs. The numbers represent the distances between the N atom (or C atom) and the surface (unit: Å). (**B**, **C**) Step-by-step hydrogenation mechanism of phenylacetylene to phenylethane on the (**B**) $PdCd_{0.5}$ (220) surface and (**C**) $PdCd_{1.25}$ (220) surface. Numbers in parentheses indicate the barriers of elementary steps. Cd, yellow; Pd, blue; C, gray; H, white.

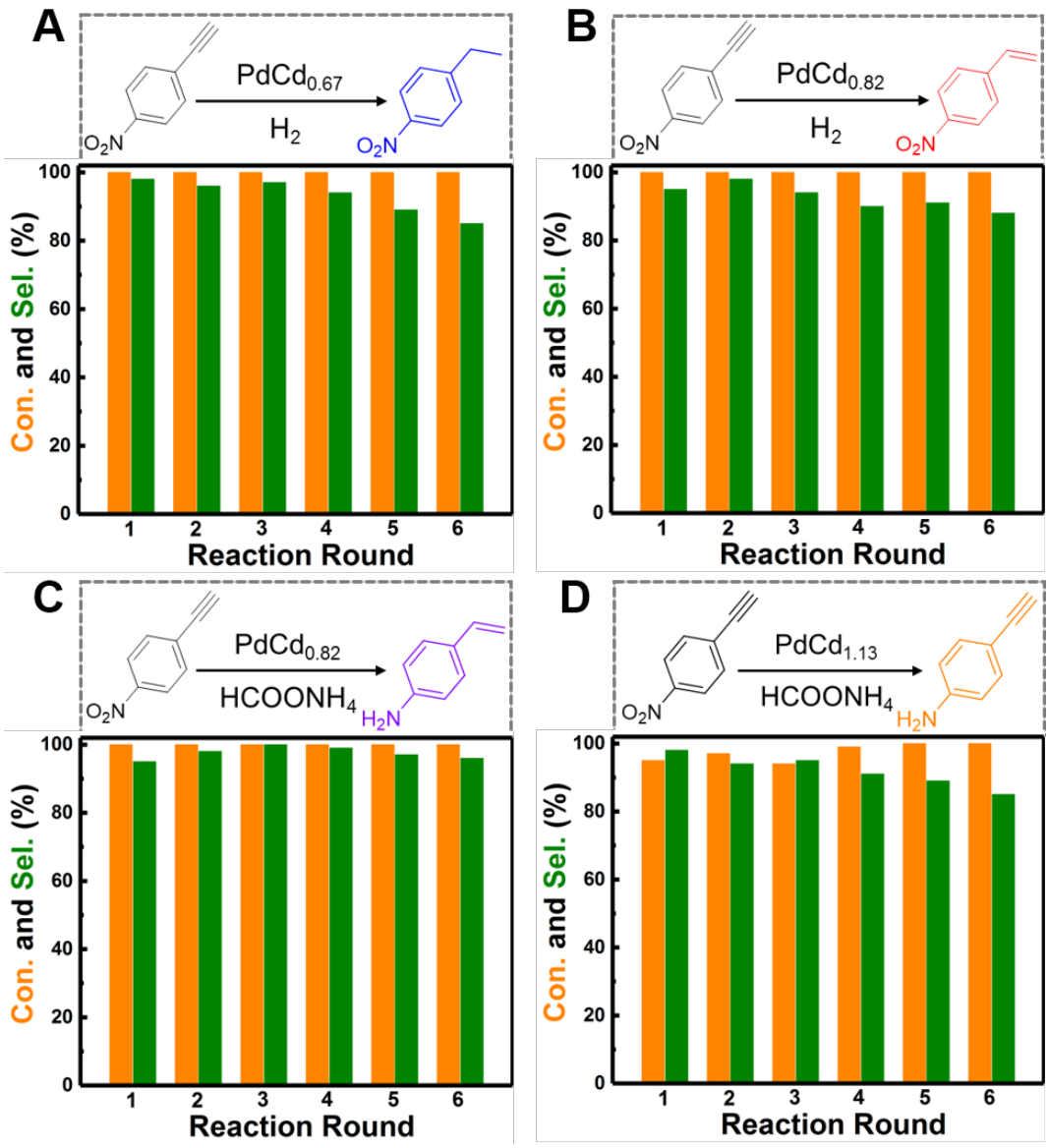

Fig. 5 The reusability of $PdCd_x$ NCs. The consecutive hydrogenation reactions of NPA over (**A**) $PdCd_{0.67}$ NCs and (**B**) $PdCd_{0.82}$ NCs using H_2 as the hydrogen source. The consecutive hydrogenation reactions of NPA over (**C**) $PdCd_{0.82}$ NCs and (**D**) $PdCd_{1.13}$ NCs using $HCOONH_4$ as the hydrogen source. The reaction time is 2 h for each run.